ENZYME CATALYSIS AND REGULATION:

Molecular Basis for Severe Epimerase Deficiency Galactosemia: X-RAY STRUCTURE OF THE HUMAN V94M-SUBSTITUTED UDP-GALACTOSE 4-EPIMERASE

James B. Thoden, Travis M. Wohlers, Judith L. Fridovich-Keil and Hazel M. Holden

J. Biol. Chem. 2001, 276:20617-20623.
doi: 10.1074/jbc.M101304200 originally published online March 7, 2001

THE JOURNAL OF BIOLOGICAL CHEMISTRY
Vol. 276, No. 23, Issue of June 8, pp. 20617–20623, 2001

Printed in U.S.A.

Molecular Basis for Severe Epimerase Deficiency Galactosemia

X-RAY STRUCTURE OF THE HUMAN V94M-SUBSTITUTED UDP-GALACTOSE 4-EPIMERASE*

Received for publication, February 9, 2001
Published, JBC Papers in Press, March 7, 2001, DOI 10.1074/jbc.M101304200

James B. Thoden‡, Travis M. Wohlers§¶, Judith L. Fridovich-Keil‖, and Hazel M. Holden‡**

From the ‡Department of Biochemistry, University of Wisconsin, Madison, Wisconsin, 53706 and the §Graduate Program in Genetics and Molecular Biology and ‖Department of Genetics, Emory University School of Medicine, Atlanta, Georgia 30322

Galactosemia is an inherited disorder characterized by an inability to metabolize galactose. Although classical galactosemia results from impairment of the second enzyme of the Leloir pathway, namely galactose-1-phosphate uridylyltransferase, alternate forms of the disorder can occur due to either galactokinase or UDP-galactose 4-epimerase deficiencies. One of the more severe cases of epimerase deficiency galactosemia arises from an amino acid substitution at position 94. It has been previously demonstrated that the V94M protein is impaired relative to the wild-type enzyme predominantly at the level of V_{max} rather than K_m. To address the molecular consequences the mutation imparts on the three-dimensional architecture of the enzyme, we have solved the structures of the V94M-substituted human epimerase complexed with NADH and UDP-glucose, UDP-galactose, UDP-GlcNAc, or UDP-GalNAc. In the wild-type enzyme, the hydrophobic side chain of Val^{94} packs near the aromatic group of the catalytic Tyr^{157} and serves as a molecular "fence" to limit the rotation of the glycosyl portions of the UDP-sugar substrates within the active site. The net effect of the V94M substitution is an opening up of the Ala^{93} to Glu^{96} surface loop, which allows free rotation of the sugars into nonproductive binding modes.

Galactosemia is a rare, potentially lethal genetic disease that is inherited as an autosomal recessive trait and results in the inability of patients to properly metabolize galactose (1). Clinical manifestations include intellectual retardation, liver dysfunction, and cataract formation, among others. Although deficiencies of any of the three enzymes participating in the Leloir pathway for galactose metabolism (Scheme 1) can result in symptoms of galactosemia, the classical form of the disease arises from impairment of galactose-1-phosphate uridylyltransferase, the second enzyme in the pathway (1).

Of particular interest is the third enzyme in the pathway, namely UDP-galactose 4-epimerase, hereafter referred to as epimerase. This NAD^+-dependent enzyme plays a key role in normal galactose metabolism by catalyzing the interconversion of UDP-galactose and UDP-glucose as indicated in Scheme 1. Interestingly, the human form of epimerase has also been shown to interconvert UDP-GlcNAc and UDP-GalNAc (2–4). This type of activity has not been observed in the epimerase from *Escherichia coli*.

Two types of human epimerase-based galactosemia have been identified thus far: peripheral and generalized. While the peripheral form can be quite common among some ethnic groups and is usually considered benign, the generalized form of the disease is clinically severe and extremely rare (5–8). The most severe form of epimerase deficiency galactosemia characterized to date arises from a homozygous mutation encoding the substitution of a methionine residue for a valine at position 94 (9). This substitution impairs enzyme activity to ~5% of wild-type levels with respect to UDP-galactose and to ~25% of wild-type levels with respect to UDP-GalNAc (10). The mutant protein is impaired relative to the wild-type enzyme predominantly at the level of V_{max} rather than K_m (10).

Previous biochemical analyses on the epimerase from *E. coli* have suggested that its reaction mechanism proceeds through abstraction of the hydrogen from the 4′-hydroxyl group of the sugar by a catalytic base and transfer of a hydride from C-4 of the sugar to C-4 of the NAD^+, leading to a 4′-ketopyranose intermediate and NADH (11). A limited but well-defined rotation of this intermediate is thought to occur in the active site, thereby allowing return of the hydride from NADH to the opposite side of the sugar. Recently, the three-dimensional structure of human epimerase complexed with NADH and UDP-glucose was solved by x-ray crystallographic analyses to 1.5-Å resolution (12). A ribbon representation of one subunit of the homodimeric protein is displayed in Fig. 1. As can be seen, the overall fold of the enzyme can be described in terms of two structural motifs: the N-terminal domain defined by Met^1–Thr^{189} and the C-terminal region formed by Gly^{190}–Ala^{348}. The N-terminal domain adopts the three-dimensional architecture referred to as a Rossmann fold. Strikingly, the NADH and UDP-glucose ligands are positioned within the active site such that C-4 of the sugar lies at ~3.5 Å from C-4 of the dinucleotide (12). Additionally, O^{η} of Tyr^{157} and O^{γ} of Ser^{132} are located at 3.1 Å and 2.4 Å, respectively, from the 4′-hydroxyl group of the sugar moiety. It is believed that the low barrier hydrogen bond formed between the sugar and the side chain of Ser^{132} facilitates the removal of the 4′-hydroxyl hydrogen by the phenolic acid chain of Tyr^{157} and the transfer of the hydride from C-4 of the sugar to C-4 of the nicotinamide ring (12).

To address the molecular consequences of the V94M substitution in human epimerase, we have crystallized and solved

* This work was supported in part by National Institutes of Health (NIH) Grants DK47814 (to H. M. H.) and DK46403 (to J. L. F-K.). Use of the Argonne National Laboratory Structural Biology Center beamlines at the Advanced Photon Source was supported by the United States Department of Energy, Office of Energy Research, under contract W-31-109-ENG-38. The costs of publication of this article were defrayed in part by the payment of page charges. This article must therefore be hereby marked "*advertisement*" in accordance with 18 U.S.C. Section 1734 solely to indicate this fact.

The atomic coordinates and structure factors (code 1I3M, 1I3N, 1I3K, and 1I3L) have been deposited in the Protein Data Bank, Research Collaboratory for Structural Bioinformatics, Rutgers University, New Brunswick, NJ (http://www.rcsb.org/).

¶ Supported in part by funds provided by NIH Predoctoral Training Grant GM08490.

** To whom correspondence should be addressed. Tel.: 608-262-4988; Fax: 608-262-1319; E-mail: Hazel_Holden@biochem.wisc.edu.

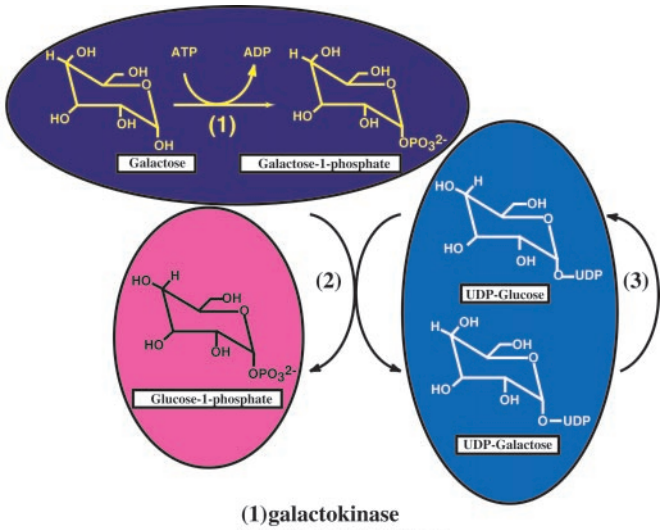

SCHEME 1

the x-ray structures of the mutant protein complexed with UDP-glucose, UDP-galactose, UDP-GlcNAc, or UDP-GalNAc, all to 1.5-Å resolution. These investigations have allowed for a more complete understanding of the three-dimensional consequences this mutation imparts on the active site geometry of the enzyme and provide a molecular explanation for the observed enzymatic impairment.

EXPERIMENTAL PROCEDURES

Crystallization of the Epimerase (V94M Mutant)·NADH·UDP-sugar Ternary Complexes—The V94M form of human UDP-galactose 4-epimerase was constructed and overexpressed in the yeast *Pichia pastoris*, as described (9, 12). Protein samples employed for crystallization trials were purified according to the protocol of Ref. 12. Ternary complexes of the protein were prepared by treating the epimerase samples (15 mg/ml in the final dialysis buffer) with 5 mM NADH and 20 mM UDP-sugars and allowing the solutions to equilibrate for 24 h at 4 °C. Large crystals of each of the complexes were grown from 100 mM MES[1] (pH 6.0), 8–9% (w/v) poly(ethylene glycol) 3400, and 75 mM $MgCl_2$ by macroseeding into batch experiments at 4 °C. Typically, the crystals grew to maximum dimensions of 0.3 × 0.2 × 0.7 mm in ~1–2 weeks.

X-ray Structural Analyses of the Ternary Complexes—For x-ray data collection, the crystals were transferred to cryoprotectant solutions in two steps. First they were slowly transferred to intermediate solutions containing 20% poly(ethylene glycol) 3400, 500 mM NaCl, and 20% (v/v) methanol. After equilibration in the methanol-containing solutions, the crystals were subsequently transferred into similar solutions that had been augmented with 4% (v/v) ethylene glycol. All of the crystals were suspended in loops of 20-μm surgical thread and immediately flash-frozen in a stream of nitrogen gas.

The four V94M protein·NADH·UDP-sugar complexes crystallized in the space group $P2_12_12_1$ with typical unit cell dimensions of a = 78.1 Å, b = 89.9 Å, and c = 96.9 Å. Each asymmetric unit contained one dimer, and only subunit I in the coordinate file will be discussed under "Results and Discussion." Native x-ray data sets to 1.5-Å resolution were collected at the Advanced Photon Source, Structural Biology Center beamline 19-BM. These data were processed with HKL2000 and scaled with SCALEPACK (13). Relevant x-ray data collection statistics are presented in Table I. The V94M protein·NADH·UDP-glucose structure was solved via AMORE (14), employing the previously determined wild-type protein·NADH·UDP-glucose structure as the search model (12). The other three structures were solved via difference Fourier techniques. Manual adjustments of the models using the program Turbo (15) and subsequent least squares refinements with the package TNT (16) reduced the R-factors to 17.5, 18.1, 18.5, and 17.8%, respectively, for the ternary complexes with UDP-glucose, UDP-galactose, UDP-GlcNAc, or UDP-GalNAc. Relevant refinement statistics can be found in Table II. Figs. 1, 2, 3, and 5 were prepared with the software package, MOLSCRIPT while Fig. 4 was generated with the program BobScript (17, 18).

[1] The abbreviation used is: MES, 2-(*N*-morpholino)ethanesulfonic acid.

RESULTS AND DISCUSSION

Recent biochemical studies on the human V94M-substituted UDP-galactose 4-epimerase revealed that the enzyme was kinetically impaired relative to the wild-type protein predominantly at the level of V_{max} rather than K_m (10). Specifically, the K_m values for the wild-type and mutant forms of the protein, when assayed with UDP-galactose, were 0.27 ± 0.01 and 0.15 ± 0.02 mM, respectively. The V_{max} values, however, were significantly different for the wild-type and V94M proteins at 1.22 *versus* 0.036 mmol of UDP-galactose/mg/min, respectively. Additionally, the apparent K_m values for the wild-type and V94M enzymes, with UDP-GalNAc as the substrate, corresponded to 0.287 ± 0.05 mM and 0.445 ± 0.01 mM, respectively.

For the x-ray investigation presented here, four different crystal forms of the V94M enzyme were prepared, namely the complexes of protein with NADH and the following ligands: UDP-glucose, UDP-galactose, UDP-GlcNAc, or UDP-galNAc. All of the structures were solved to 1.5-Å resolution and refined to R-factors equal to or less than 18.5%. The relative location of the galactosemic mutation with respect to the active site of the native enzyme can be seen in Fig. 2*a*. As expected, the main structural perturbation imposed by the V94M substitution occurs in the helical loop defined by Ala^{93} to Glu^{96}, which connects the fourth β-strand to the fourth major α-helix of the Rossmann fold. This change in loop structure is similar in all of the V94M protein models described here and is independent of the identity of the sugar ligand occupying the active site. In the wild-type enzyme, the side chain of Val^{94} points toward the active site and is located at ~3.5 Å from the catalytic Tyr^{157}. Additionally, the carbonyl oxygen of Val^{94} forms a hydrogen bond with the side chain hydroxyl group of Ser^{97}, which further serves to tighten down that portion of the polypeptide chain backbone abutting the UDP-sugar binding pocket. This loop in the wild-type enzyme is well ordered with an average temperature factor of 22.0 $Å^2$ for all of the atoms lying between Ala^{93} and Glu^{96}. The corresponding temperature factors for the V94M protein·NADH·UDP-sugar complexes are significantly higher, however, at ~77 $Å^2$. Indeed, residual electron density in maps calculated with $(F_o - F_c)$ coefficients suggests that alternate conformations of this loop are present in the crystalline lattice but at lower occupancies. It was not possible to build these alternate conformations into the electron density with any certainty, however, and hence they were not included in the protein models.

A superposition of the polypeptide chains near residue 94 for the wild-type enzyme and the V94M protein complexed with UDP-galactose is displayed in Fig. 2*b*. The mutation at position 94 results in a significant change in the backbone dihedral angles of the preceding alanine residue. Specifically, in the wild-type enzyme, Ala^{93} adopts ϕ and ψ angles of approximately −82 and 106°, respectively, while in the V94M protein, the corresponding angles are −124° and 148°. As a result of these changes in torsional angles, the side chain of Met^{94} in the mutant protein extends out toward the solvent, and the hydrogen bond between the carbonyl oxygen of residue 94 and O^{γ} of Ser^{97} is no longer present. It should be noted that if the loop between Ala^{93} and Glu^{96} were to adopt the wild-type conformation in the V94M protein, the larger side chain of Met^{94} could not be accommodated in the active site without significant steric clashes, and this, presumably, explains in part the dramatic changes in backbone conformation starting at position 93.

The net effect of this three-dimensional perturbation is an

TABLE I
X-ray data collection statistics

	Resolution	Independent reflections	Completeness	Redundancy	Avg I/Avg $\sigma(I)$	R_{sym}[a]
	Å		%			%
Protein · NADH · UDP-glucose	50.0–1.50	108,994	99.1	6.7	41.0	4.7
	1.55–1.50[b]	10,333	95.3	3.8	3.5	23.9
Protein · NADH · UDP-galactose	50.0–1.50	107,566	97.4	6.6	40.0	5.5
	1.55–1.50	9406	86.0	3.7	3.3	24.0
Protein · NADH · UDP-GlcNAc	50.0–1.50	107,985	98.4	6.4	34.4	5.8
	1.55–1.50	9535	88.0	3.6	2.5	27.6
Protein · NADH · UDP-GalNAc	50.0–1.50	107,214	97.3	7.0	37.9	5.3
	1.55–1.50	9400	86.2	4.2	3.0	27.9

[a] $R_{sym} = (\Sigma|I - \bar{I}|/\Sigma I) \times 100$.
[b] Statistics for the highest resolution bin.

TABLE II
Relevant least-squares refinement statistics

Bound ligand	UDP-glucose	UDP-galactose	UDP-GlcNAc	UDP-GalNAc
Resolution limits (Å)	30.0–1.50	30.0–1.50	30.0–1.50	30.0–1.50
R-factor[a] (overall) %/reflections	17.5/108,668	18.1/107,191	18.5/107,692	17.8/107,109
R-factor (working) %/reflections	17.4/97,801	18.1/96,472	18.4/96,922	18.0/96,398
R-factor (free) %/reflections	19.8/10,687	20.3/10,719	21.4/10,770	21.5/10,711
No. of Protein Atoms[b]	5413	5414	5388	5403
No. of Hetero-atoms[c]	1155	1107	1014	1097
Weighted root mean square deviations from ideality				
Bond lengths (Å)	0.010	0.010	0.012	0.010
Bond angles (degrees)	2.10	2.21	2.14	2.17
Trigonal planes (Å)	0.005	0.005	0.005	0.005
General planes (Å)	0.009	0.011	0.011	0.012
Torsional angles (degrees)	15.6	15.8	15.6	15.7

[a] R-factor = $(\Sigma|F_o - F_c|/\Sigma|F_o|) \times 100$ where F_o is the observed structure-factor amplitude and F_c is the calculated structure-factor amplitude.
[b] These include multiple conformations for 1) UDP-Glu: Glu^{24}, Glu^{63}, and Ser^{81} in subunit I and Ser^{59}, Glu^{61}, Ser^{81}, Met^{83}, Lys^{120}, Thr^{134}, Thr^{177}, Ile^{217}, Asp^{231}, Glu^{233}, Ile^{252}, and Ser^{342} in subunit II; 2) UDP-galactose: Glu^{24}, Glu^{63}, Ser^{81}, Thr^{189}, and Asn^{207} in subunit I and Glu^{24}, Glu^{63}, Gln^{114}, Lys^{120}, Thr^{134}, Thr^{177}, Thr^{189}, Ile^{217}, and Gln^{261} in subunit II; 3) UDP-GlcNAc: Glu^{24}, Glu^{63}, and Asn^{138} in subunit I and Glu^{61}, Ile^{118}, Thr^{134}, Thr^{177}, and Asn^{207} in subunit II: 4) UDP-GalNAc: Lys^{120} and Arg^{256} in subunit I and Glu^{3}, Glu^{24}, Gln^{114}, Ile^{118}, Thr^{134}, Asn^{207}, Asp^{231}, and Gln^{282} in subunit II.
[c] These include for 1) UDP-glucose: 2 NADH, 2 UDP-glucose, 4 Cl^-, 1 Mg^{2+}, 3 ethylene glycols, and 977 waters; 2) UDP-galactose: 2 NADH, 2 UDP-galactose, 3 Cl^-, 1 Mg^{2+}, 2 ethylene glycols, and 935 waters; 3) UDP-GlcNAc: 2 NADH, 2 UDP-GlcNAc, 4 Cl^-, 1 Mg^{2+}, and 842 waters; 4) UDP-GalNAc: 2 NADH, 1 UDP-GlcNAc, 1 UDP-GlcNAc, 4 Cl^-, 1 Mg^{2+}, and 925 waters.

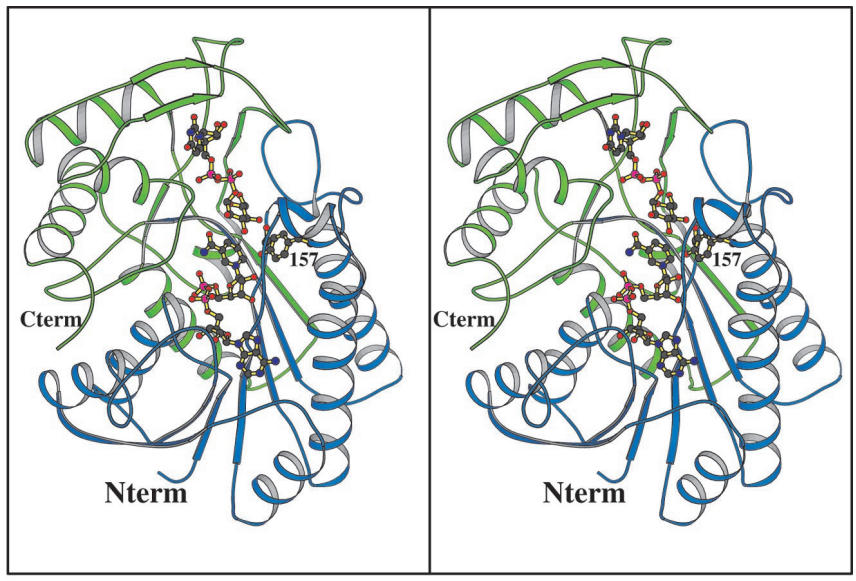

FIG. 1. **Ribbon representation of one subunit of human UDP-galactose 4-epimerase.** X-ray coordinates employed for this *figure* were solved by this laboratory and can be obtained from the Protein Data Bank (Research Collaboratory for Structural Bioinformatics, Rutgers University, New Brunswick, NJ) (1EK6). Bound UDP-glucose and NADH are displayed in ball-and-stick representations. Both Ser^{132} (not labeled) and the catalytic Tyr^{157} are also shown.

opening of the active site, thereby allowing free rotation of the sugar moiety. Indeed, from electron density maps calculated with $(F_o - F_c)$ coefficients, it is clear that the sugars in the V94M structures complexed with either UDP-glucose or UDP-galactose adopt multiple conformations that are not well defined. Because of this, it is not possible to describe in detail the carbohydrate/protein interactions in these two particular structures. It is possible, however, to compare the interactions between the protein and the UDP moieties in the wild-type and the V94M proteins with either bound UDP-glucose or UDP-galactose. Potential hydrogen-bonding interactions observed between the wild-type enzyme and the substrate are depicted in a schematic representation in Fig. 3*a*, while those for the V94M·NADH·UDP-glucose complex are shown in Fig. 3*b*. As indicated, the side chains forming hydrogen bonds to the UDP-glucose in the wild-type protein include Ser^{132}, Tyr^{157}, Asn^{187},

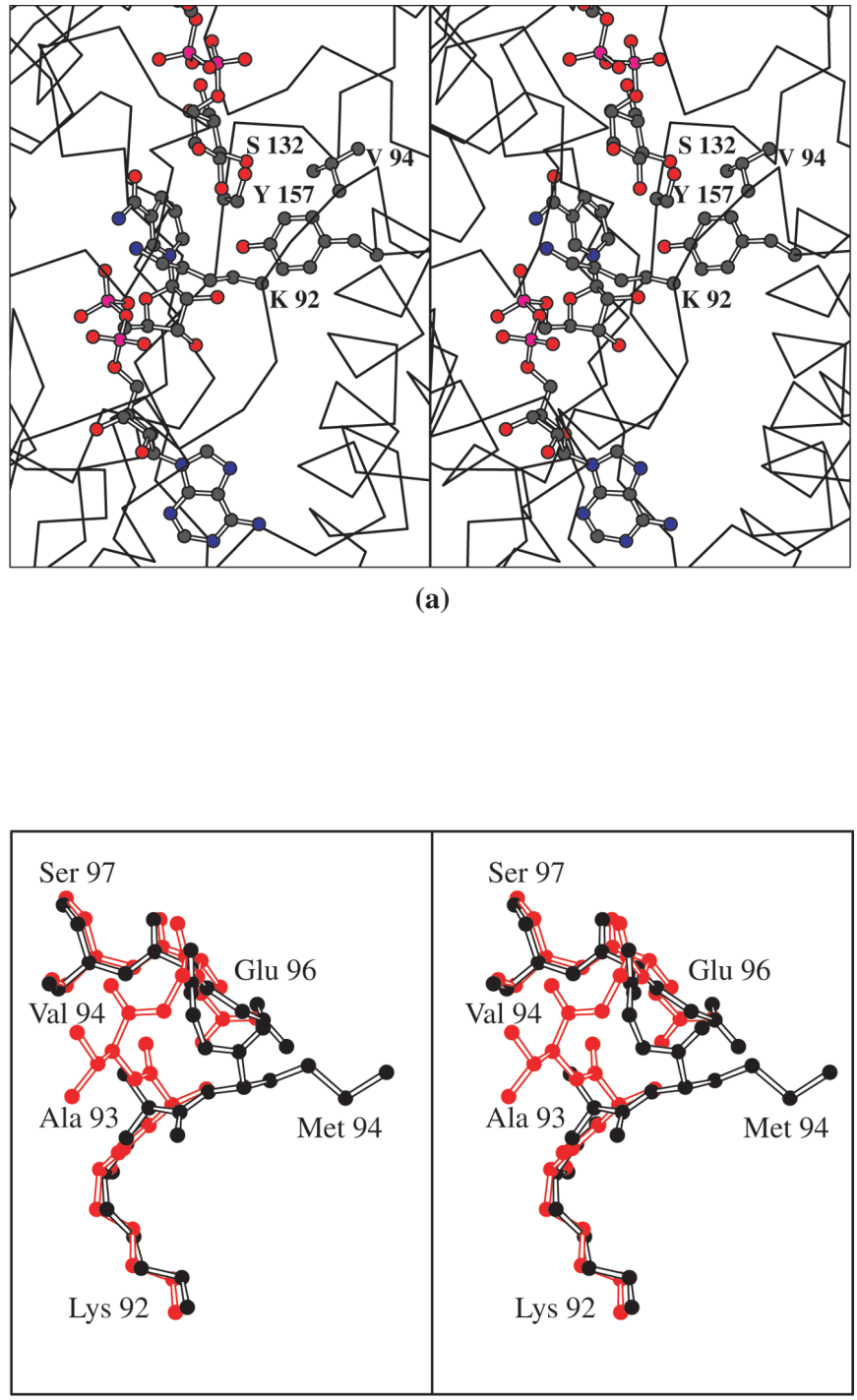

FIG. 2. **Location of the V94M mutation that results in severe epimerase deficiency galactosemia.** The relative location of position 94 with respect to the active site in the wild-type enzyme is shown in *a*. A superposition of the wild-type and V94M polypeptide chains near the mutation is given in *b*. The wild-type enzyme is displayed in *red*, while the V94M protein is drawn in *black*.

Asn^{207}, Arg^{239}, Asp^{303}, and Arg^{300}. Only Ser^{132} and Tyr^{157} interact solely with the carbohydrate portion. All of the other side chains are primarily involved in UDP binding. As can be seen in Fig. 3*a*, the uracil ring of the UDP-glucose is anchored to the native enzyme via the backbone carbonyl group of Asn^{224} and the peptidic NH group of Phe^{226}. Two additional water molecules serve to bridge the C-4 carbonyl group of the base to the protein. These interactions are also observed in the various V94M mutant protein models (Fig. 3*b*). In the wild-type protein, the 2′- and 3′-hydroxyl groups of the uridine ribose are hydrogen-bonded to the carboxylate group of Asp^{303} and a water molecule, respectively. The guanidinium group of Arg^{300} interacts with both α- and β-phosphoryl oxygens of UDP when bound to wild-type enzyme, while the side chain of Arg^{239} forms an electrostatic interaction with a β-phosphoryl oxygen. Similar interactions are, indeed, observed in the V94M enzymes as indicated in Fig. 3*b*. The only significant differences between the wild-type enzyme and the V94M protein occur at the glucose moiety. In the wild-type protein, the glucose moiety is firmly anchored in place by interactions with the side chains of Ser^{132} and Tyr^{157} and the carbonyl oxygen of Lys^{92}, which is located in the loop containing the V94M mutation. These interactions are missing in the mutant proteins with bound UDP-glucose or UDP-galactose due to the free rotation of the glycosyl groups in the active site. The limited change in K_m observed between the wild-type enzyme and the V94M protein is a func-

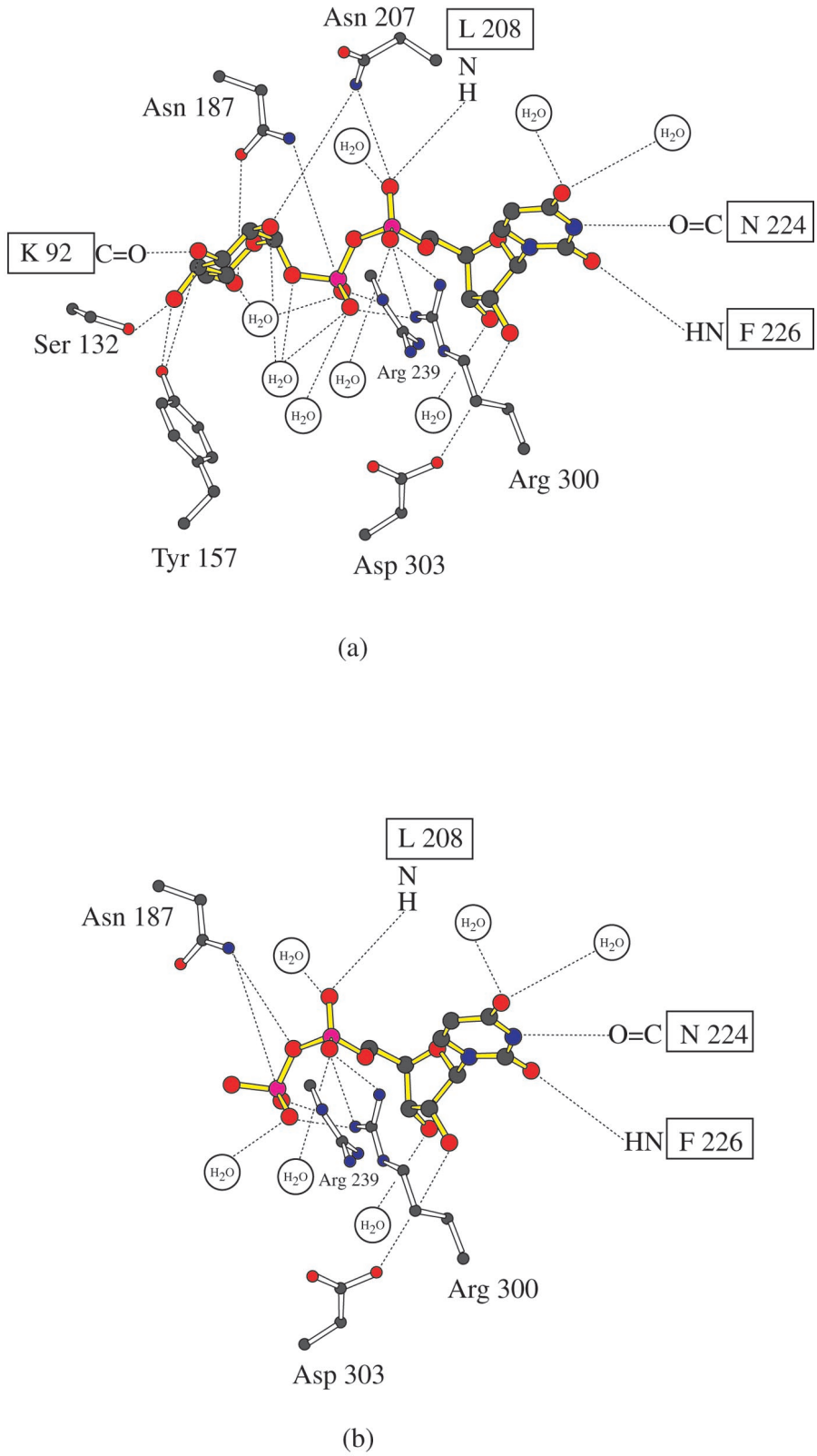

FIG. 3. **Comparison of the hydrogen bonding patterns around the UDP when bound to either the wild-type enzyme or the V94M protein.** Possible electrostatic interactions between the native enzyme and the UDP-glucose ligand are indicated by the *dashed lines* in *a*. The UDP-glucose is highlighted in *yellow bonds* for clarity. The *dashed lines* indicate distances equal to or less than 3.2 Å. Interactions between the V94M protein and the UDP (in the V94M·NADH·UDP-glucose model) are indicated (*b*). The sugar moiety is not shown due to its free rotation in the active site of the V94M-substituted epimerase.

tion of the fact that the nucleotide portion of the UDP-sugar substrate provides most of the binding interactions.

Unlike that observed for the V94M protein·NADH·UDP-glucose or the V94M protein·NADH·UDP-galactose complexes, the sugar moieties in the V94M proteins with either bound UDP-GlcNAc or UDP-GalNAc are visible in the electron density maps as shown in Fig. 4 for the UDP-GlcNAc species. Note that the 6′-hydroxyl group of the *N*-acetylglucosamine adopts two conformations and that the sugar is rotated away from the nicotinamide ring of the NADH. Residual electron density in maps calculated with $(F_o - F_c)$ coefficients suggests that each of these sugars adopt alternate conformations at lower occupancies. Because of the quality of the residual electron density, however, it was not possible to unambiguously model these alternate conformations into the electron density; hence, they were not included in the coordinate files.

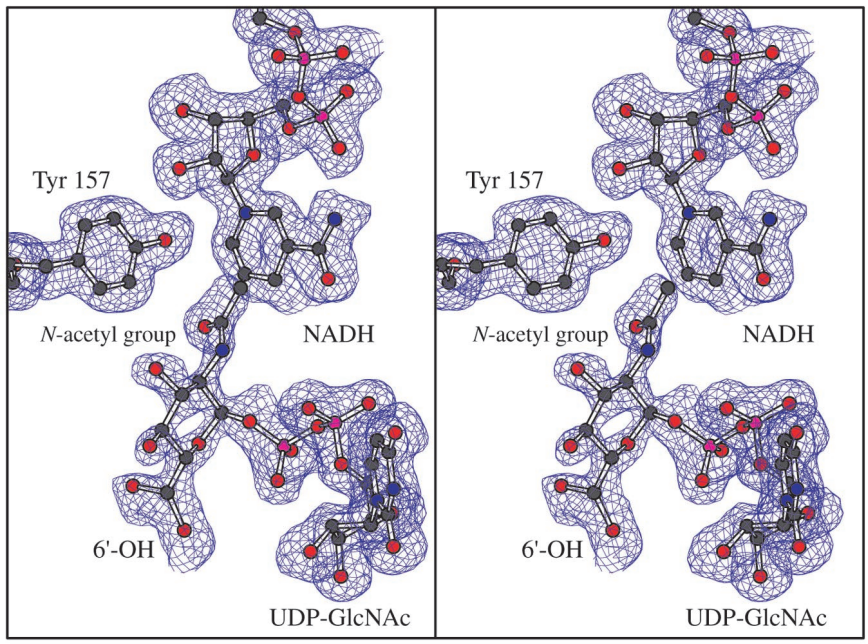

FIG. 4. **Electron density in the vicinity of the UDP-GlcNAc binding pocket.** The map was contoured at 2σ and calculated with coefficients of the form $(F_o - F_c)$, where F_o was the native structure factor amplitude and F_c was the calculated structure factor amplitude. The UDP-GlcNAc ligand, the NADH, and Tyr^{157} were omitted from the x-ray coordinate file for the electron density map calculation.

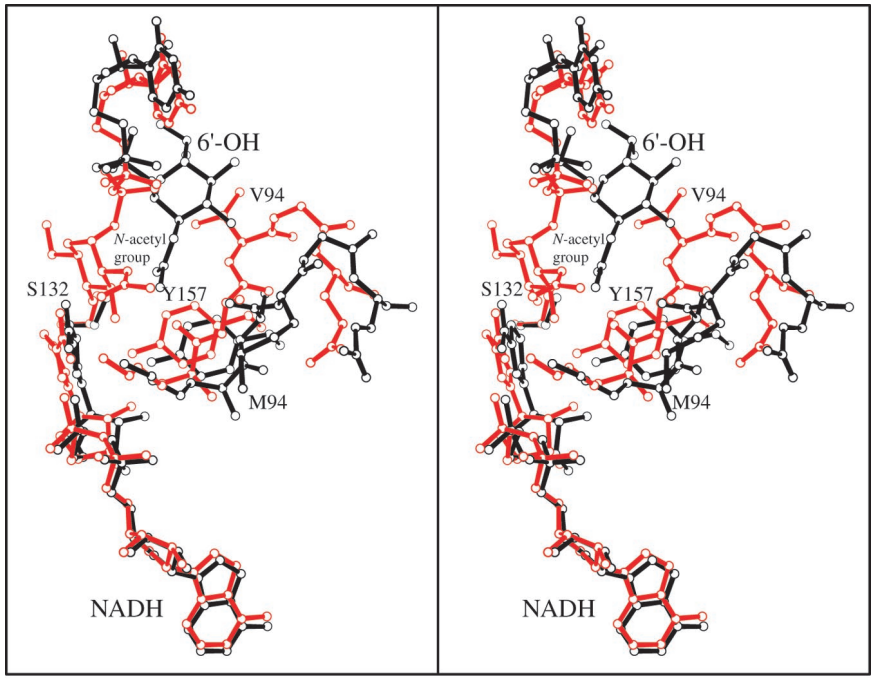

FIG. 5. **Superposition of the regions near the active sites for the abortive complexes of wild-type enzyme and the V94M protein with bound UDP-GlcNAc.** The wild-type and V94M proteins are depicted in *red* and *black*, respectively. Note the significant rotation of the *N*-acetylglucosamine moiety out of the active site pocket in the V94M protein.

Interestingly, the electron density map calculated for the V94M enzyme crystallized in the presence of UDP-GalNAc clearly demonstrated that the ligand had been converted to UDP-GlcNAc. This result is reminiscent of that observed with the epimerase from *E. coli*. All attempts to prepare an abortive complex of the bacterial enzyme with UDP-galactose failed (19). These experiments included reduction of the enzyme with dimethylamine/borane in the presence of UDP-galactose, UDP, UMP, or TMP and subsequent exchange of these nucleotides with UDP-galactose. In every case, the electron density maps always indicated the presence of UDP-glucose in the active site. Obviously, UDP-glucose binds more tightly to epimerase in the abortive complex, and although the enzyme had been reduced with dimethylamine/borane, enough residual activity remained to convert UDP-galactose to UDP-glucose. Most likely, the same phenomenon is occurring in the case of the human V94M-substituted epimerase with bound UDP-GalNAc.

Within the last year, the three-dimensional structure of human wild-type epimerase with bound NADH and UDP-GlcNAc was solved to 1.5-Å resolution, and it was demonstrated that to accommodate the additional *N*-acetyl group at the C-2 position of the sugar, the side chain of Asn^{207} rotates toward the interior of the protein and interacts with Glu^{199} (20). Shown in Fig. 5 is a superposition of the active site regions for the wild-type and V94M proteins with bound UDP-GlcNAc. As can be seen, in the V94M-substituted form, the sugar group of the ligand rotates out of the pocket and toward position 94. This type of rotation is blocked in the native enzyme due to the side chain of Val^{94}. In the wild-type enzyme the distance between C-4 of the UDP-GlcNAc ligand and C-4 of the nicotinamide ring of the NADH is 3.0 Å. This distance in the V94M protein model is 9.4 Å. The 4′-hydroxyl group of the sugar in the wild-type enzyme is

located at 2.8 Å from O^{γ} of Ser^{132} and 3.0 Å from O^{η} of Tyr^{157}. Due to the drastic rotation of the sugar moiety in the active site pocket, these distances in the V94M protein complex are 9.5 and 10.2 Å, respectively. Key hydrogen bonds between the *N*-acetylglucosamine group of the ligand and the wild-type enzyme occur between the side chains of Asn^{187} and the 6′-OH of the sugar, between both Ser^{132} and Tyr^{157} and the 4′-OH of the sugar, and finally, between the carbonyl group of Lys^{92} and the 3′-OH of the carbohydrate. These interactions are completely missing in the V94M enzyme with bound UDP-GlcNAc, where the hydroxyl groups simply form hydrogen bonds with solvent molecules.

In summary, the x-ray studies described here provide a three-dimensional understanding of one example of severe epimerase deficiency galactosemia. In the normal enzyme, the hydrophobic side chain of Val^{94} provides a "molecular fence" to prevent sugar rotation out of the active site pocket, thereby preventing nonproductive binding. Upon substitution of Val^{94} by a methionine, the loop region connecting the fourth β-strand to the fourth α-helix of the Rossmann fold becomes disordered, adopts multiple conformations, and effectively opens up the sugar binding pocket to allow for free rotation of the sugar moiety in the active site and/or nonproductive substrate binding. In light of the structural results presented here, it is not surprising that the V94M mutation effects V_{max} significantly more than K_m. Most of the binding interactions for the UDP-sugar substrates occur between the protein and the nucleotide, and these are not disrupted by the mutation. What the V94M substitution does, however, is allow the carbohydrate portions of the UDP-sugars to rotate freely, thereby limiting the time the ligand is bound in a productive mode near O^{γ} of Ser^{132} and O^{η} of Tyr^{157}. As such, V_{max} is severely affected. Interestingly, in previous work, it has been shown that the V94M epimerase is impaired to a 5-fold lesser extent with regard to UDP-GalNAc than to UDP-galactose (9). The reason is, presumably, that the bulkier sugar moieties of UDP-GlcNAc and UDP-GalNAc can adopt fewer nonproductive binding modes.

Acknowledgments—We are grateful to Drs. Dale Edmondson and Paige Newton-Vinson for generously allowing and helping us to use the fermenter and to Dr. W. W. Cleland for helpful discussions.

REFERENCES

1. Holton J. B., Walter J. H., Tyfield L. A. (2000) in Metabolic and Molecular Bases of Inherited Disease (Scriver, C. R., Beaudet, A. L., Sly, S. W., and Valle, D., eds) 8th Ed., pp. 1553–1587, McGraw-Hill, New York
2. Maley, F., and Maley, G. F. (1959) *Biochim. Biophys. Acta* **31,** 577–578
3. Piller, F., Hanlon, M. H., and Hill, R. L. (1983) *J. Biol. Chem.* **258,** 10774–10778
4. Kingsley, D. M., Kozarsky, K. F., Hobbie, L., and Krieger, M. (1986) *Cell* **44,** 749–759
5. Gitzelmann, R. (1972) *Helv. Paediatr. Acta* **27,** 125–130
6. Gitzelmann, R., and Steinmann, B. (1973) *Helv. Paediatr. Acta* **28,** 497–510
7. Gitzelmann, R., Steinmann, B., Mitchell, B., and Haigis, E. (1977) *Helv. Paediatr. Acta* **31,** 441–452
8. Alano, A., Almashanu, S., Maceratesi, P., Reichardt, J., Panny, S., and Cowan, T. M. (1997) *J. Invest. Med.* **45,** 191 (abstr.)
9. Wohlers, T. M., Christacos, N. C., Harreman, M. T., and Fridovich-Keil, J. L. (1999) *Am. J. Hum. Genet.* **64,** 462–470
10. Wohlers, T. M., and Fridovich-Keil, J. L. (2000) *J. Inherit. Metab. Dis.* **23,** 713–729
11. Frey, P. A. (1987) in *Pyridine Nucleotide Coenzymes: Chemical, Biochemical, and Medical Aspects* (Dolphin, D., Poulson, R., and Avramovic, O., eds) p. 461, John Wiley & Sons, Inc., New York
12. Thoden, J. B., Wohlers, T. M., Fridovich-Keil, J. L., and Holden, H. M. (2000) *Biochemistry* **39,** 5691–5701
13. Otwinowski, Z., and Minor, W. (1997) *Methods Enzymol.* **276,** 307–326
14. Navaza, J. (1994) *Acta Crystallogr. A* **50,** 157–163
15. Roussel, A., and Cambillau, C. (1991) *Silicon Graphics Geometry Partners Directory*, Silicon Graphics, Mountain View, CA
16. Tronrud, D. E., Ten Eyck, L. F., and Matthews, B. W. (1987) *Acta Crystallogr. Sect. A.* **43,** 489–501
17. Kraulis, P. J. (1991) *J. Appl. Crystallogr.* **24,** 946–950
18. Esnouf, R. (1996) *BobScript*, version 2.01, *J. Appl. Cryst.* (1991) **24,** 946–950
19. Thoden, J. B., Frey, P. A., and Holden, H. M. (1996) *Biochemistry* **35,** 5137–5144
20. Thoden, J. B., Wohlers, T. M., Fridovich-Keil, J. L., and Holden, H. M. (2001) *J. Biol. Chem.* **276,** 15131–15136